

## 6 Application perspectives of intense laser pulses in atmospheric diagnostics

Wiebke Zimmer, Miguel Rodriguez and Ludger Wöste

### 6.1 Introduction

Since many years lasers have been used in atmospheric diagnostics, especially in remote sensing. In particular the lidar method (described in the previous sections) has become a powerful technique to monitor atmospheric parameters and has helped to understand a variety of atmospheric phenomena.

In the field of laser research, on the other hand, the generation of ultra-short laser pulses made the decisive step forward with the development of the chirped pulse amplification (CPA) technique in 1985 [1,2]. It opened the way to light pulses with peak power values exceeding  $10^{12}$  W and to enormous short-time intensities.

Both aspects together suggest to evaluate, if the application of high-intensity lasers can improve existing techniques or create new methods in atmospheric diagnostic, i.e. for remote sensing. The outstanding new aspect thereby is that the air, which is matter composed of gases and particles, i.e. aerosols, plays a double role. It is not only the object of analysis, but also a medium on which the possible measuring methods are based. Extremely non-classic light-matter interactions promise new possibilities for atmospheric science, but, to be able to interpret the measurements correctly, they also require intensive investigations which belong to the current basic research in quantum optics.

The state of these investigations, including first results of laboratory experiments as well as measurements in the atmosphere, will be presented in the following sections. Beforehand, a short introduction in the high-power laser technique and the basic effects of nonlinear optics is given.

#### ***Generation of ultra-short high-intensity laser pulses***

The active laser medium commonly used for the generation of short pulses is the titanium-doped sapphire crystal which has a very broad gain bandwidth ( $\sim 700$  to  $1000$  nm). Its optimal activation frequency lies in the green spectral region, therefore powerful Nd:YAG lasers, emitting at a wavelength of  $532$  nm (frequency doubled), are applied as pump lasers. In the CPA technique an initial short pulse, e.g. with a duration of some tens of femtoseconds ( $\sim 10^{-14}$  s) generated by a

modelocked Ti:Sa oscillator, is first temporally stretched in order to reduce its peak power. In this way it can be amplified without damaging the optics, passing through a series of amplifier stages containing the same active medium as the oscillator. The amplified pulse is finally recompressed to nearly its original duration. In both, stretcher and compressor, gratings are used to control the pulse duration. The temporal expansion is therefore a consequence of the separation of the different colors in the pulse spectrum, the so-called *chirping* of the pulse. This is possible because of the fact that the initial pulse, due to its temporal sharpness, has a broad spectrum, typically of the order of 30 nm full width half maximum (FWHM).

Today commercial CPA systems with output energies of several hundreds of millijoules are available. With pulse durations of about 100 fs these systems provide a peak power of several terawatts ( $10^{12}$  W). For laboratory experiments as described in section 6.3 also femtosecond laser systems of lower pulse energies (in the order of 1 mJ) can serve to create the required light intensities. Laser systems of that kind are used by many research groups, e.g. in chemical physics.

### **Nonlinear optics**

When a high power laser pulse propagates through a transparent medium it undergoes nonlinear self-action effects which lead to strong changes of the spectral, temporal and spatial characteristics of the pulse. Those phenomena have been extensively studied since the early 1970s [3].

A basic principal of nonlinear optics is the variation of the refractive index of matter in the presence of strong electro-magnetic fields. For a given radiation frequency the refractive index  $n$ , which is no more a constant of the medium, depends in the form

$$n = n_0 + n_2 I \text{ (+ higher terms),} \quad (6.1)$$

on the light intensity  $I$ , where  $n_0$  is the linear refractive index and  $n_2$  is the coefficient of the nonlinear refractive index. In the case of a high-power laser beam the transverse intensity profile, e.g. gaussian or  $\text{sech}^2$ , leads to a higher refractive index in the centre of the beam than at the edge, inducing a so-called Kerr lens. The result is a self-focusing [4,5] of the beam, causing a further increase of intensity. If the light appears as short pulses, the variation of the refractive index on the longitudinal axis, due to the trailing and the falling edge of the pulse, is also important. The resulting self-phase modulation [3,6] changes, i.e. broadens, the pulse spectrum, while temporal effects like self-steepening and pulse splitting [7] may occur. In addition to the  $n_2$  effects, multi-photon processes, as the generation of high harmonics, four-wave mixing or multi-photon ionization (MPI), take place at very high intensities.

Nonlinear propagation of laser beams in matter is known as long as the laser itself and it could first be observed in solid media, i.e. crystals. Some well known nonlinear effects like frequency doubling or tripling are specifically related to the anisotropic structure of crystals. But only the development of ultra-short pulse lasers permitted to observe nonlinear effects even in gases at atmospheric pressure.

## 6.2 Interaction of intense laser pulses with air – detection of gases

### *Propagation and white-light generation*

The  $n_2$  coefficient (see eq. 6.1) of air is quite difficult to retrieve experimentally. We assume a value of  $5 \times 10^{-19} \text{ cm}^2/\text{W}$  at 800 nm which leads to a self-focusing threshold power of 2 GW for a refraction limited beam. In this section we deal with terawatt laser pulses, exceeding by far this threshold. As a typical example, the self-focusing length for a 3-TW pulse at 800 nm with a beam diameter of 5 cm is, in theory, approximately 60 m.

When the intensity of the self-focusing beam reaches a certain threshold, the light starts to generate a plasma because of MPI. From that point on the presence of free charges lowers the refractive index which, in contrast to the Kerr lens effect, causes a defocusing of the beam. A balance of both effects leads to an outstanding phenomenon of nonlinear propagation called self-guiding or self-channelling [8]. Generally, TW-pulses are not focused to one plasma channel but are converted into a bundle of filaments (see Fig. 6.1). Single-filament guiding is achieved with lower laser power and/or very “clean” beam profiles. The guiding can be stable over very long paths compared to the length of a “classic” focal region. Filaments of up to 200 m in length have been reported [9]. The diameter of such filaments is about  $100 \mu\text{m}$  and the critical intensity of self-guided filaments is estimated to lie between  $10^{13}$  and  $10^{14} \text{ W/cm}^2$  for 800-nm pulses [10], slightly above the threshold for multi-photon ionisation (MPI).

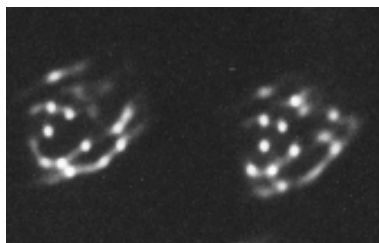


**Fig. 6.1.** Photograph of filament patterns of two consecutive self-focusing TW-pulses after 50 m of propagation in air (each whole-beam diameter is approx. 5 cm).

Inside those filaments the spectral shape of the pulse is strongly modified. The most striking change is visible to the naked eye: the infrared beam converts into white light (note that Fig. 6.1 is a real photograph of a scattering screen). This phenomenon is called supercontinuum generation (SCG) [11]. Recently such spectra, which maintain their maximum at the laser wavelength ( $\sim 800 \text{ nm}$ ), have been measured between the UV and the mid-IR. White light could be detected from  $150 \text{ nm}$  to  $4.5 \mu\text{m}$  [12]. Self-phase modulation (SPM) is believed to be the main source of the continuum, but it is influenced by other effects, mainly MPI and the group velocity dispersion (GVD), which is a linear effect but has special

relevance for ultra-short pulses. Emission of the low-density plasma produced in gases by filamentation plays a minor role. This may be different when the gas, e.g. air, contains aerosols (see section 6.3). In contrast to plasma emission, the white light generated in coherent processes, like SPM or four-wave mixing, is forward directed [13].

There are different approaches to successful modelling of filamentation and SCG, but a complete theory is still lacking. Numerical simulations are still limited by enormous computing times and have only been performed for short distances. Therefore long-distance propagation experiments (see the “Outlook” section 6.4) are needed, in general for an understanding of the physics, but also for the application of high-power femtosecond lasers to analyse the atmosphere.

### ***Femtosecond white-light lidar: remote atmospheric spectroscopy***

The main advantage of lidar over other remote sensing techniques, as differential optical absorption spectroscopy DOAS or fourier transform infrared spectroscopy FTIR (both using natural or artificial white-light sources), is the high spatial resolution over long distances, which is achieved by the use of short laser pulses and fast electronics to record the signal of the backscattered light. A terawatt laser can serve as a fast-pulsed highly collimated white-light source for lidar. In first experiments to evaluate this possibility [14] the laser-like divergence of the white light was verified by detecting the backscattered light from 12-km high cirrus clouds. Therefore a self-focusing 2-TW 790-nm laser beam was used measuring only the light between 350 and 650 nm (BG39 filter).

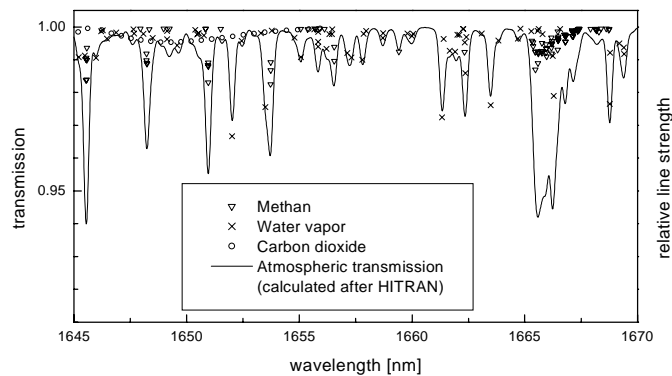


**Fig. 6.2.** Simulated absorption spectrum of 3 km atmosphere under normal conditions. The line-by-line calculation of the spectrum (solid line) implies an experimental resolution of 0.25 nm. The symbols indicate the relative oscillator strength (a.u.) of the single absorption lines (disregarding weak lines). Line data have been taken from HITRAN 2000 [15].

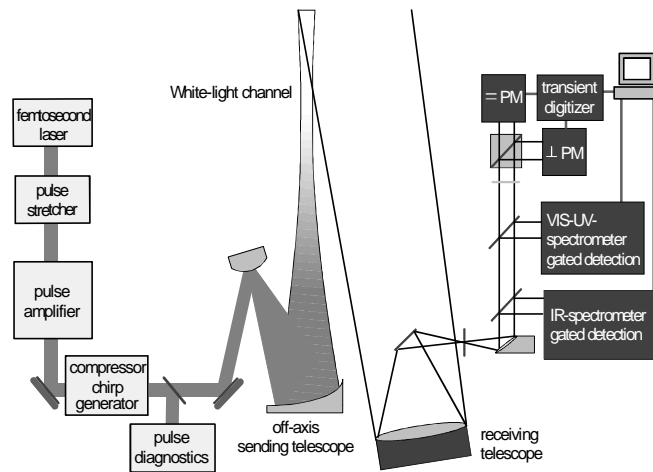


**Fig. 6.3.** Schematic setup of the femtosecond white-light lidar.

The near to mid-IR is of great interest in atmospheric science, because many pollutant and climate relevant gases, e.g. the volatile organic compounds (VOC) have strong absorption bands in this spectral region. Great efforts are undertaken in the development of (tunable) lasers which cover this wavelength range. But taking into account that, in contrast to typical UV absorption bands, in the IR the molecules have narrow absorption lines in bands which strongly overlap with those of other molecules (Fig. 6.2), it is easier to measure precisely the absorption with a light continuum than with monochromatic lasers. Even if the spectrum can not be measured in full resolution (the natural line-widths determined by atmospheric pressure and Doppler broadening) exact fitting of the data is possible, while using monochromatic lasers the spectral shape and exact position of the laser line for the measurement is very critical.

A highly collimated pulsed white-light source, as terawatt lasers now provide, does not only offer the mentioned advantages for the retrieval of gas concentrations, but could also become a real multi-component lidar for the simultaneous detection of various gases. This would be very much acclaimed by the modelist. Although a limitation still lies in the availability of suitable detectors for the infrared, particularly multi-channel devices. If a single-point detector has to be used in a scanning process, the measurement is very time-consuming, as it would be using a continuously tunable laser.

The schematic setup of the femtosecond white-light lidar with a multi-spectral detection is shown in Fig. 6.3. An example of a measured water vapour spectrum and the fitting of the calculated absorption is shown in Fig. 6.4. In this experiment, where a 2-TW 790-nm laser was used, the H<sub>2</sub>O mixing ratio could be obtained with an estimated accuracy of 15% [16]. The uncertainty was mainly due to a lack of knowledge about the distance at which the white-light is created. In this regard further experiments dedicated to the study of SCG are needed.

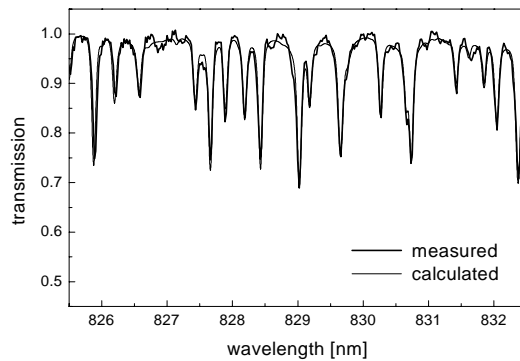


**Fig. 6.4.** Absorption spectrum of water vapour (normalized). The backscatter signal from 600-1000 m height was measured with a multi-channel analyzer. The humidity (mixing ratio of  $\text{H}_2\text{O}$ ) is retrieved through a fit to the calculated spectrum (based on HITRAN).

The laser parameters can be set to optimise the SCG in filaments, e.g. through a slight initial focusing of the beam with an adjustable sending telescope. A special feature is the so called negative pre-chirp: in order to compensate the GVD the faster components of the spectrum are set to the back of the initial pulse by tuning the pulse compressor (see section 6.1). In this way the intensity can be enhanced at a certain distance and the position of the filaments can be shifted. This fact might have a huge impact on lidar, because an enhanced backscatter of light by the air in the filament region was recently demonstrated in laboratory experiments [17].

### 6.3 Interaction of intense laser pulses with microdroplets – characterization of aerosols

A further step in the evaluation of new lidar techniques, beyond the ones described in the previous section, lies in the interaction of intense laser pulses with atmospheric aerosols. In this context the question arises, if there are nonlinear optical effects which can provide information about the composition of aerosols. To address this issue in detail it is important to study at first the interaction of femtosecond laser pulses with microdroplets in laboratory experiments: Which nonlinear optical effects can be generated in droplets and are their size and their chemical composition determinable. Particularly, with regard to a possible lidar application, the angular dependence of the emitted light is of major interest. It would be a great advantage, if the angular intensity distribution favored the backscatter direction due to anisotropic scattering. Therefore an experimental arrangement is presented which conforms to the described requirements. Then the most important nonlinear optical effects of the interaction of intense laser pulses with microdroplets will be discussed.

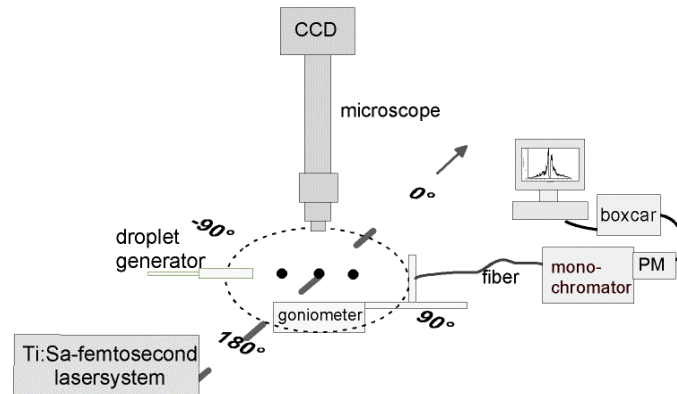


**Fig. 6.5.** Schematic setup for the measurement of the spectral and angular distribution of the light emitted by microdroplets, due to the interaction with femtosecond laser pulses.

### **Experimental setup**

The schematic experimental setup is given in Fig. 6.5. An amplified Ti:Sa femtosecond laser system generates light pulses with a repetition rate of 1 kHz, a pulse duration of 80 fs and a central wavelength of 810 nm. A TOPAS (travelling-wave optical parametric amplifier) allows to access a spectral range from 800 nm to 1600 nm. A piezo driven nozzle produces single droplets with a range in diameter from 30 to 50  $\mu\text{m}$ . The droplet diameter can be modified by the amplitude and duration of the driving pulse of the nozzle and is continuously monitored by a combination of a microscope and a CCD-Camera. Under fixed conditions the droplet diameter is found to be constant with a drop to drop variation of less than 2%. The droplet generation is synchronized to the laser system and the femtosecond pulses are focused on the droplets using a 20 mm-focal length lens. The setup permits to vary the intensity between  $10^{11}$  and  $10^{13}$   $\text{W}/\text{cm}^2$ . To observe the angular dependence of the emitted light, an optical fiber is mounted on a goniometer which has its centre directly under the point of interaction. This arrangement allows an angular range from  $-60^\circ$  to  $178^\circ$  to be used. The  $0^\circ$ -position is defined to be the forward direction of the laser beam. The emitted light is guided to a grating-spectrometer and is detected by a photomultiplier tube (PM). To reduce the noise, the PM-signal passes a boxcar averager module with an integration window of about 30 ns duration and an average over 100 laser shots. This arrangement allows to perform two types of measurements:

- the angular dependence of the scattered light intensity at one particular wavelength
- the spectrum of the emitted light at one defined angle.

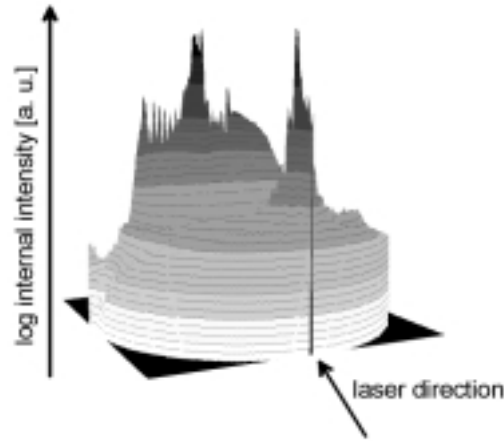


**Fig. 6.6.** 3-dimensional logarithmic illustration of the relative internal intensity in the equatorial plane of a droplet with a diameter of 55  $\mu\text{m}$  and a refractive index of 1.329 excited by a femtosecond laser pulse.

### ***Nonlinear optical effects in microdroplets***

Microdroplets are attractive systems for the study of several nonlinear optical effects. In microspheres the intensity required for such processes is much lower than in the macroscopic volume due to their strongly curved liquid-air interface. It acts as a lens and focuses the incident radiation on some small regions inside the droplet. At these areas of high intensity the efficiency for nonlinear optical processes is strongly enhanced.

With Lorenz-Mie-theory the scattering of a planar electromagnetic wave at an homogeneous spherical particle can be described [18, 19]. The scattered wave and the internal intensity distribution depend only on the refractive index of the droplet medium and on the size parameter, which is the ratio of the droplet diameter to the wavelength of the incident light. In case of the interaction of femtosecond laser pulses with microdroplets the properties of ultra short laser pulses have to be taken into account. An ultra short laser pulse has a large spectral bandwidth. Therefore a large size parameter range has to be considered calculating the internal intensity distribution of the incident light in the droplet by Mie-theory. From the 3-dimensional illustration of this intensity distribution in the equatorial plane of a sphere it is clearly visible, that the droplet concentrates the internal field at some regions, the so called hot spots (Fig. 6.6). At these points the efficiency for nonlinear optical processes is enhanced and depends strongly on the order of the process.

### High Harmonic Generation

Among the nonlinear optical effects coherent and incoherent processes have to be distinguished. Coherent nonlinear optical processes like third harmonic generation (THG) and sum frequency generation in microdroplets are well studied using picosecond laser pulses [20, 21]. THG was also observed to be the most efficient nonlinear optical effect induced by femtosecond laser pulses in water droplets [22]. Spectral analysis of the light emitted by water droplets show no higher harmonic of even order, as expected due to the inversion symmetry of liquids. Only at the surface of the droplet this symmetry is broken enabling the oriented molecules at the interface liquid-air to generate an even order polarisation. In pure water droplets the intensity of the second harmonic generated at the surface is very low [23], but it was observed in water droplets coated with surfactant molecules [24]. Odd harmonics however were measured up to the fifth harmonic generated by femtosecond infrared laser pulses [25]. The inset in Fig. 6.7 (left) shows the VIS-spectrum of the light emitted by a water droplet with a diameter of 55  $\mu\text{m}$  excited at 810 nm and a pulse intensity of  $3.5 \cdot 10^{11}$  W/cm<sup>2</sup>. The intense THG signal at 270 nm is clearly visible. The angular distribution of the third harmonic radiation is given in Fig. 6.7 (left). It shows a maximum in forward direction between 0° and 42° which is strongly modulated. Backward scattering is hardly detectable. By decreasing the size parameters the pattern simplifies. For smaller size parameter a model was developed using the standard Green function [26]. The spatial and angular distribution of THG can be calculated assuming that the THG results from the surface and the interior of the droplet. In Fig. 6.7 (right) the experimental result and the calculation for a size parameter of 80 are compared and show a remarkable agreement. The fifth harmonic indicates nearly the same angular behaviour [25].

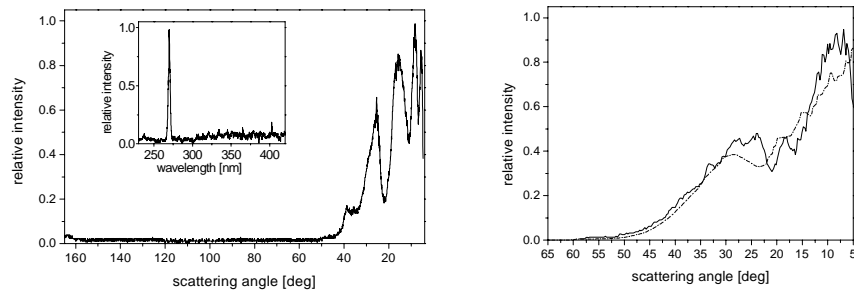


**Fig 6.7.** Left: Angular distribution of the THG-intensity generated in a water droplet with a diameter of 55  $\mu\text{m}$ , excited by a pump wavelength of 810 nm. Inset: Generated light in the UV-VIS region at a scattering angle of 30°. Right: Angular distribution of the THG-intensity of the experiment (solid) [25] and theory (dashed) [26] for a size parameter of 80.

### Multi-Photon-Fluorescence

In contrast, incoherent nonlinear optical effects can have an angular intensity distribution enhanced in the backscatter direction. The fluorescence of an ensemble of freely rotating molecules for example is isotropic. But when these molecules are homogeneously embedded in a microdroplet, the emission can become anisotropic. Since the sphere concentrates the incident radiation at certain regions an angular dependent re-emission is initiated. Due to the reciprocity principle the fluorescence radiation returns of regions of high intensity to the light source [27]. The intensity of the fluorescence  $U_n(\vartheta_d)$  which is detected at an angle  $\vartheta_d$  is the sum of the contributions from all molecules in the droplet of volume  $V$

$$U_n(\vartheta_d) = \int_V \sigma_n I_{\text{int}}^n(\vec{r}) \rho_0 [F(\vec{r}, \vartheta_n)] dV \quad (6.2)$$

where  $\sigma_n$  is the n-photon-absorption cross-section,  $I^{\text{int}}(\vec{r}) = \vec{E}^{\text{int}}(\vec{r}) \vec{E}^{\text{int}*}(\vec{r})$  is the internal intensity of the incident wave,  $\rho_0$  is the molecule density and  $F(\vec{r}, \vartheta_n)$  the probability that a photon emitted from a molecule at the position  $\vec{r}$  is detected [28].  $F(\vec{r}, \vartheta_n)$  and  $I^{\text{int}}(\vec{r})$  have to be integrated both, the spectral bandwidth of the laser pulse and the spectral bandwidth of the fluorescence. In the measurements reported, ethanol and methanol droplets containing the dye coumarin 510 were used. The central wavelength of the pump was 400 nm, 850 nm and 1200 nm. This corresponds to a 1-, 2- and 3-photon-excitation. As an example Fig. 6.8 shows a 3-photon-fluorescence. Both the calculation and the experimental results show an enhanced backscatter. These enhancement increases with the number of photons [29].

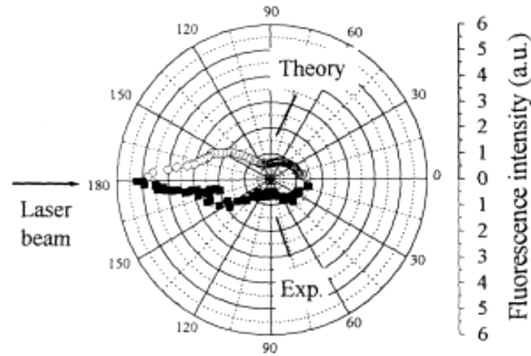


**Fig. 6.8.** Experimental and theoretical angular distribution of the emission of a 3-photon-fluorescence process induced in a microdroplet containing coumarin 510 [29].

### **Laser-induced breakdown**

By the interaction of femtosecond laser pulses with water droplets the intensity is high enough to initiate a laser induced breakdown. Due to multi-photon-ionisation a plasma is generated in the regions of high intensity inside the droplet [30]. The plasma creation within a nominally transparent droplet transforms it into a highly absorbing droplet. Once breakdown has occurred and plasma has been generated in this volume the remaining portion of the laser pulse is absorbed raising the temperature and the pressure of the volume to very high values. Plasma temperatures of 30,000 K and pressures up to 500,000 atm in droplets were observed and calculated [31]. Since the internal-field distribution and the laser-induced plasma distribution are nonuniform the explosive vaporisation is asymmetrical relative to the droplet centre. This behaviour is illustrated in Fig. 6.9 for two different laser intensities. The images are taken with a CCD camera illuminated with an LED during an exposure time of 400 ns. By varying the delay between the time of laser-droplet-interaction and the illumination the distorted droplets are imaged with time resolution. The internal heating is greatest just within the shadow face and it is clearly visible that the local high pressure causes expansion. The droplet breaks open at the shadow side and a jet stream is ejected away from the droplet. At higher intensities this process is much more pronounced, the shock wave traverses the droplet also in the opposite direction and vapour is streaming additionally from the illuminated side. In less than 70 ns the droplet is completely vaporized.

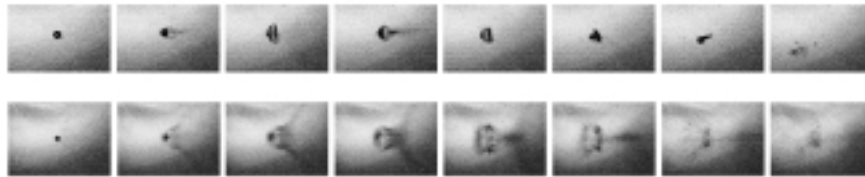


**Fig. 6.9.** Photographical sequences of the interaction of femtosecond laser pulses with microdroplets. The droplet diameter is 30  $\mu\text{m}$ , and the laser propagates from the left to the right side. First sequence with a laser intensity of  $10^{12}$   $\text{W}/\text{cm}^2$  represents the droplet with a delay of 0 ns, 700 ns, 1400 ns, 1800 ns, 8700 ns, 12000 ns, 20700 ns and 69700 ns. Second sequence with a laser intensity of  $9,7 \cdot 10^{12}$   $\text{W}/\text{cm}^2$  represents the droplet with a delay of 0 ns, 500 ns, 1100 ns, 1700 ns, 3000 ns, 5900 ns and 7100 ns.

### **Plasma emission**

The heated plasma produces a luminescence spectrum, which include two types of radiation. On one hand it acts as a source of a continuum, the emission of bremsstrahlung and electron-ion-recombination. Using the Planck equation the plasma temperature can be estimated [32]. For the white-light spectrum generated in water droplets with a laser intensity of  $1,7 \cdot 10^{15}$   $\text{W}/\text{cm}^2$ , as shown in Fig 6.10, the estimated temperature is 7300 K.

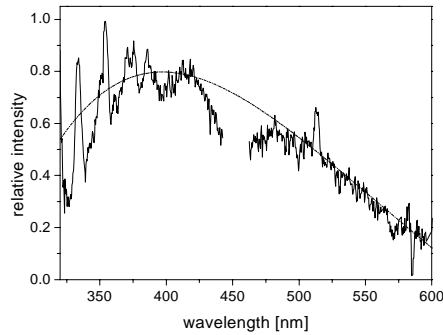


**Fig. 6.10.** Spectrum of the light emitted by a water droplet at a scattering angle of  $12^\circ$  by an excitation intensity of  $1.7 \cdot 10^{15} \text{ W/cm}^2$ . Due to the high intensity of the laser pulses the droplet generation was irregular. Therefore the spectrum shows intensity fluctuation. The dashed line represents the black body radiation at a temperature of 7300 K.

On the other hand there are emissions of electronic transitions. Normally these emissions have completely different temporal and spectral characteristics than the continuum emission. They have spectrally narrow peaks and their frequency and life time are significant for the excited species. The lifetime of these excited states are orders of magnitude longer than the duration of a femtosecond laser pulse. And the emission starts not until the background radiation decayed [33]. The weak  $\alpha$ - and  $\beta$ - Balmer lines of hydrogen could be observed in the ns-regime [34]. The  $H_\alpha$ -lines were used to determine the electron density and the plasma temperature was calculated by the intensity ratio of the  $H_\alpha$ - and  $H_\beta$ -lines [35, 36]. The observation of these plasma lines - also known as laser induced breakdown spectroscopy (LIBS) - represents an attractive method in the research of atmospheric aerosols, since these aerosols mainly consist of water containing additional substances [37], which can be identified by their plasma lines. For example, the sea salt aerosol contains sodium chloride. Sodium has two strong emission bands around 589 nm. If water droplets containing 5-M sodium chloride solution are excited by laser pulses starting at an intensity of  $4 \cdot 10^{14} \text{ W/cm}^2$ , an orange flash is even visible with the naked eye. The spectrum of the emitted light, detected at a scattering angle of  $165^\circ$ , is displayed in Fig. 6.11. The sodium signal is so intense that the white light continuum disappears in the background noise [38]. Due to the Stark effect the doublet is not resolvable [39]. The angular distribution of the 589 nm peak shows a strong enhancement in backscatter direction, a finding which opens fascinating prospects for atmospheric remote sensing.

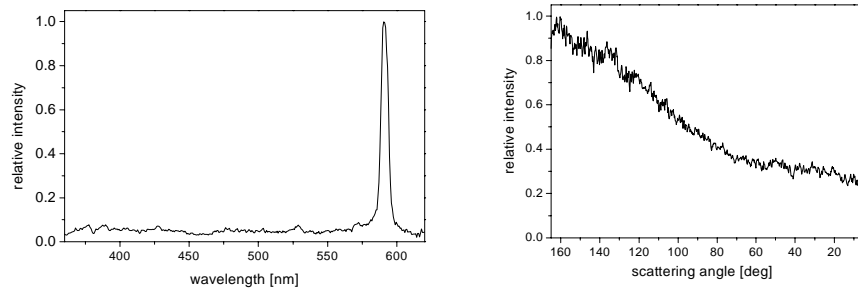


**Fig. 6.11.** Left: Spectrum of the light emitted in  $165^\circ$  direction by a microdroplet containing a 5 molar NaCl solution. Right: Angular distribution of the 598 nm signal. Laser intensity:  $7.2 \cdot 10^{14}$  W/cm<sup>2</sup>.

## 6.4 Outlook

Until now all the described results have been obtained using lasers that are stationed in laboratories. Recently, the first mobile terawatt laser has been designed and built in the framework of a French-German research project called Teramobile [40]. A 5-TW laser was integrated in a standard freight container, together with detection optics and electronics for lidar. The Teramobile only requires a power supply, which can be a generator. It contains air condition and an autonomous cooling system for the laser and the electrical devices. This mobile laboratory will allow to fulfil the mentioned requirements and to investigate out the possibilities for in field analysis of the atmosphere:

- Long-distance propagation experiments will be performed on free plane sites, e.g. former air fields. In that way horizontal scanning of the laser beam over ranges of several kilometres will be possible.
- The system can be brought to nearly any place, so that the new lidar techniques can be performed under different atmospheric conditions.
- Experiments with aerosols will be done under real and defined artificial conditions. Field measurements can, on one hand, be dedicated to the study of the propagation of TW pulses in a simulated cloud or haze of water droplets, to observe how the presence of particles modifies the filament formation. On the other hand, experiments will evaluate the potential of measuring aerosol compositions based on the results described in section 6.3.

## References

1. Strickland D, Mourou G (1985) Compression of amplified chirped optical pulses. *Opt Commun* 56: 219
2. Backus S, Durfee CG III, Murnane MM, Kapteyn HC (1998) High power ultrafast lasers. *Rev Sci Instrum* 69: 1207-1223
3. Alfano RR, Shapiro SL (1970). *Phys Rev Lett* 24: pp 584, 592, 1217
4. Shen Y (1984) *The principles of nonlinear optics*. Wiley, New York
5. Strickland D, Corkum PB (1994) Resistance of short pulses to self-focusing. *J Opt Soc Am B* 11: 492
6. Manassah JT(1989) Simple Models of Self-Phase and Induced-Phase Modulation, in Ref. 11
7. Ranka JK, Schirmer RW, Gaeta AL (1996) Observation of Pulse Splitting in Nonlinear Dispersive Media. *Phys Rev Lett* 77: 3783
8. Braun A, Korn G, Liu X, Du D, Squier J, Mourou G (1995) Self-channeling of high-peak-power femtosecond laser pulses in air. *Opt Lett* 20: 73
9. La Fontaine B, Vidal F, Jiang Z, Chien CY, Comtois D, Desparois A, Johnson TW, Kieffer JC, Pépin H (1999) Filamentation of ultrashort pulse laser beams resulting from their propagation over long distances in air, *Phys Plasmas* 6: 1615-1621
11. Alfano RR (ed, 1989) *The Supercontinuum Laser Source*. Springer, Berlin Heidelberg New York
12. Kasparian J, Sauerbrey R, Mondelain D, Niedermeier S, Yu J, Wolf JP, André YB, Franco M, Prade B, Mysyrowicz A, Tzortzakis S, Rodriguez M, Wille H, Wöste L (2000) Infrared extension of the supercontinuum generated by fs-TW-laser pulses propagating in the atmosphere. *Opt Lett* 25: 1397-1399
13. Chin SL, Petit S, Borne F, Miyazaki K (1999) The white light supercontinuum is indeed an ultrafast white light laser. *Jpn J Appl Phys* 38: L126-L128
14. Wöste L, Wedekind C, Wille H, Rairoux P, Stein B, Nikolov S, Werner C, Niedermeier S, Ronneberger F, Schillinger H, Sauerbrey R (1997) Femtosecond atmospheric lamp. *Laser und Optoelektronik* 29: 51
15. Rothman LS et al. (1998) The HITRAN molecular spectroscopic database and HAWKS (HITRAN atmospheric workstation), 1996 edition. *J Quant Spectrosc Radiat Transfer* 60: 665-710 (see [www.hitran.com](http://www.hitran.com) for HITRAN 2000)
16. Rairoux P, Schillinger H, Niedermeier S, Rodriguez M, Ronneberger F, Sauerbrey R, Stein B, Waite D, Wedekind C, Wille H, Wöste L (2000) Remote sensing of the atmosphere using ultrashort laser pulses. *Appl Phys B* 71: 573-580
17. Yu J, Mondelain D, Ange G, Volk R, Niedermeier S, Wolf JP, Kasparian J, Sauerbrey R (2001) Backward supercontinuum emission from a filament generated by ultrashort laser pulses in air. *Opt Lett* 26: 533-535
18. Barber PW, Hill SC (1990) *Light Scattering by Particles*. In: *Computational Method*. World Scientific, Singapore
19. Barton (1995) Internal and near surface electromagnetic fields for spheroidal particle with arbitrary illumination. *Appl Opt* 34: 5542-5551
20. Hill SC, Leach DH, Chang RK (1993) Third-order sum-frequency generation in droplets: model with numerical results for third-harmonic generation. *J Opt Soc Am B* 10: 16-33

21. Leach DH, Chang RK, Acker WP, Hill SC (1993) Third-order sum-frequency generation in droplets: experimental results. *J Opt Soc Am B* 10: 34-45
22. Kasparian J, Krämer B, Dewitz JP, Vajda S, Rairoux P, Vezin B, Boutou V, Leisner T, Hübner W, Wolf JP, Wöste L, Bennemann KH (1997) Angular Dependences of Third Harmonic Generation from Microdroplets. *Phys Rev Lett* 78: 2952-2955
23. Goh MC, Hicks JM, Pinto RG, Bhattacharyya K, Eisenthal KB, Heinz TF (1988) Absolute orientation of water molecules at the near water surface. *J Phys Chem* 92: 5074-5079
24. Hartings JM, Poon A, Pu X, Chang RK, Leslie TM (1997) Second harmonic generation and fluorescence images from surfactants on hanging droplets. *Chem Phys Lett* 281: 389-393
25. Zimmer W, Krenz M, Wöste L, Leisner T (2001) High harmonic generation in microdroplets. in preparation
26. Carrol D, Zheng XH (1998) Modelling third harmonic generation from microdroplets. *Pure Appl Opt* 7: L49-L55
27. Hill SC, Videen G, Pendleton JD (1997) Reciprocity method for obtaining the far fields generated by a source inside or near a microparticle. *J Opt Soc Am B* 10: 2522-2529
28. Hill SC, Saleheen HI, Barnes MD, Whitten WB, Ramsey JM (1996) Modeling fluorescence collection from single molecules in microspheres: effects of position, orientation, and frequency. *Appl Opt* 35: 6278-6288
29. Hill SC, Boutou V, Yu J, Ramstein S, Wolf JP, Pan Y, Holler S, Chang RK (2000) Enhanced Backward-Directed Multi-Photon-Excited Fluorescence from Dielectric Microcavities. *Phys Rev Lett* 85: 54-57
30. Hammer DX, Thomas RJ, Noojin GD, Rockwell BA, Kennedy PK, Roach WP (1996) Experimental Investigation of Ultrashort Pulse Laser-induced Breakdown Thresholds in Aqueous Media. *IEEE J Quantum Electron* 32: 670-677
31. Carls JC, Seo Y, Brock JR (1991) Laser-induced breakout and detonation waves in droplets. II Model. *J Opt Soc Am B* 8: 329-336
32. Barnes PA, Rieckhoff KE (1968) Laser induced underwater sparks. *Appl Phys Lett* 13: 282-284
33. Cremers DA, Radziemski LJ, Loree TR (1984) Spectrochemical Analysis of Liquids Using the Laser Spark. *Appl Spectrosc* 38: 721-729
34. Eickmans HE, Hsieh WF, Chang RK (1987) Laser induced explosion of H<sub>2</sub>O droplets: spatially resolved spectra. *J Opt Soc Am B* 12: 22-24
35. Griem HG (1964) *Plasma Spectroscopy*. McGraw-Hill Book Company, New York
36. Chang RK, Eickmanns JH, Hsieh WF, Wood CF, Zhang JZ, Zheng J (1988) Laser-induced breakdown in large transparent water droplets. *Appl Opt* 27: 2377-2385
37. Poulain DE, Alexander DR (1995) Influences on Concentration Measurements of Liquid Aerosol by Laser-Induced Breakdown Spectroscopy. *Appl Spectrosc* 49: 569-579
38. Zimmer W (2001) Nichtlineare optische Effekte bei der Wechselwirkung von Femtosekundenlaserpulsen mit Mikrotropfen. PhD Thesis, FU Berlin
39. Eickmans HE, Hsieh WF, Chang RK (1987) Plasma spectroscopy of H, Li, Na in plumes resulting from laser-induced droplet explosion. *Appl Opt* 26: 3721-3725
40. Wille H, Rodriguez M, Kasparian J, Mondelain D, Yu J, Mysyrowicz A, Sauerbrey R, Wolf JP, Wöste L (2001) Teramobile: a mobile femtosecond-terawatt laser and detection system. *Eur Phys J D* (submitted)